Journal of the European Ceramic Society **16** (1996) 261–267

0955-2219/96/$15.00

Processing of Mullite-based Long-fibre Composites via Slurry Routes and by Oxidation of an Al–Si Alloy Powder

J. Brandt[a] & R. Lundberg[b]

[a]Swedish Ceramic Institute, Box 5403, S-402 29 Göteborg, Sweden
[b]Volvo Aero Corporation, S-461 81 Trollhättan, Sweden

(Accepted 22 July 1995)

Abstract

A novel technique to synthesize mullite by the oxidation of Al–Si alloy powder was used for the manufacture of Al_2O_3 long-fibre reinforced mullite composites. It included (1) slurry infiltration/fibre winding of continuous Al_2O_3 yarns (ALMAX) and (2) slurry infiltration/slip casting of sapphire fibres (Saphikon). The nonaqueous slurry used consisted of an Al–Si alloy, mullite and additives. During reaction-bonding of green matrices, the Al–Si alloy oxidized and was fully converted to mullite after 1 h at 1430°C in air. The oxidation caused an internal volume expansion, resulting in reduced fibre/matrix shrinkage stresses during reaction-bonding of composites, which minimized the sensitivity to crack formations. For the ALMAX-based composites, the fracture was non-catastrophic. Regarding the sapphire-based composites, an interfacial space between the fibres and the matrix gave the desired fibre pull-out.

1 Introduction

Ceramic long-fibre reinforced composites are being considered as future materials for gas turbine hot parts.[1] However, there are still some obstacles to overcome before this group of materials are mature enough for turbine applications, where there are high demands on long-term, high-temperature stability in the oxidizing environment. For instance, it has been difficult to produce dense ceramic long-fibre composites with adequate high temperature properties, including good oxidation resistance, for use at over 1400°C. This is especially true for nonoxide materials, where both fibres, matrix and interface material are nonoxides and consequently oxidize to form a strong fibre/matrix bond leading to brittle fracture behaviour.[2] One possible solution is to develop composites consisting of high temperature *oxide* matrices and fibres and maybe even allow some open porosity in the final material.[3]

Mullite ($Al_6Si_2O_{13}$) is of particular interest as matrix material among the binary metal oxide ceramics.[4] This refractory possesses good creep resistance and excellent oxidation resistance.[5] However, the drawbacks of mullite are the low fracture toughness (K_{1c} = 2–3 MPa·m$^{1/2}$) and the poor sinterability, mainly due to the low interdiffusion rates of silicon and aluminium ions in crystalline mullite.[6] However, if this material is reinforced with high-temperature oxide long-fibres, and if some porosity could be accepted, then mullite could definitely be a competitive, moderate cost material for high-temperature structural applications. The fibres also facilitate the production of large thin-walled, complex-shaped components.[7]

A new technique to synthesize mullite has been developed, particularly, in view of the manufacture of mullite-based long-fibre composites.[8] The technique is described in this paper. In short, a mixture of an Al–Si alloy and oxide powders is milled and formed into a powder compact, after which the alloy is oxidized and reaction-bonded to its corresponding ceramic composition, i.e. mullite. The brittle Al–Si is effectively comminuted during milling, avoiding the formation of undesired large, flat agglomerates by cold welding, as is the case with pure Al powder.[9,10] Consequently, when long-fibre composites are processed, fibre tows are more easily infiltrated. Because of the fine metal distribution in the alloy, the transformation to mullite, during oxidation and reaction-bonding, is favoured. Another advantage is that the oxidation causes an internal volume expansion of the matrix.[11] This minimizes the sensitivity to crack formation due to reduced shrinkage stresses between the fibres and the matrix.[12,13]

2 Experimental

2.1 Materials

A commercially available, gas-atomized Al–Si alloy with a weight-ratio of 75:25 (Al75/Si25 (hypereutectic compound)), particle size <150 μm, (AL146010, GoodFellow, UK) was selected. The Al–Si ratio is close to the one necessary for the formation of stoichiometric mullite ($3Al_2O_3 \cdot 2SiO_2$) during reaction-bonding. Between 577 and 760°C, the Al75/Si25 alloy is melted to a liquid phase of a eutectic composition (Al88/Si18) plus a solid phase of large Si grains.[14] On oxidation, the theoretical weight increase is 95%. If full conversion to mullite is achieved (including some excess Al_2O_3), the volume expansion is 59%. In addition to the alloy, the oxide powders used were mullite (SACR193, Baikowski Chimie, France), Al_2O_3 (AKP-30, Sumitomo, Japan) and MgO (Merck, Germany) as an oxidation catalyst. Extra Al_2O_3 was added to form mullite of otherwise unreacted, free SiO_2 — an excess of Al_2O_3 was preferred in the final material.

Two kinds of ceramic long fibres were used for the manufacture of the composites: (1) polycrystalline, continuous α–Al_2O_3 yarn with 1000 filaments per yarn (filament diameter 10 μm) and without any sizing (ALMAX Y-1010S-N, Mitsui Mining Material, Japan) and (2) single crystal, continuous α–Al_2O_3 sapphire fibres with a diameter of 130 μm (Saphikon, USA). Whereas the ALMAX polycrystalline fibres showed limited resistance to heat in earlier experiments, the sapphire fibres have excellent high temperature properties.[15,16] The ALMAX fibres should thus be considered as a model material.

For the preparation of the slurry, an organic, non-polar solvent, with a high boiling point, and a suitable dispersant, KD–3 (ICI, USA), were used.

2.2 Specimen preparation

One master slurry was prepared for all the experiments. A batch with a composition by weight of 30% A175/Si25, 63% mullite, 5% Al_2O_3 and 2% MgO was mixed in the organic solvent with 3% KD–3 (on powder), resulting in a solid loading of 73·0 wt% (40·3 vol%). After prolonged ball milling, the slurry was wet-sieved through a 20 μm cloth.

Bars with the dimensions 60 × 9 × 8 mm^3 were slip cast onto a plaster mould, both with and without a few sapphire fibres suspended parallel in the middle of the mould. In addition, long-fibre composites with the ALMAX fibre yarn were prepared by slurry infiltration/fibre winding. To keep the filament together during the fibre winding procedure, the fibre yarn bobbin was soaked with organic solvent. The yarn was then passed through the slurry, with a thread tension of 0·08 N and a speed of 2 m/min, and wound on a quadrangular take-up spool (65 × 65 mm^2). When the soaked yarn came into contact with the slurry, the organic solvent had evaporated enough for the yarn, via capillary forces, to become fully impregnated by the slurry. In fact, the solvent residue improved the wettability of the yarn. All specimens were carefully dried, burned out in nitrogen at 500°C and subsequently stored in a dry atmosphere.

The specimens were reaction-bonded and partly densified in flowing air with heating rates of 10°C/min to 450°C and 2°C/min to maximum temperatures of 1430–1600°C with dwelling periods of 5–240 min.

2.3 Evaluation

The effect of ball milling was verified by means of specific surface area (BET) measurements and micrographs of the particles, before and after milling. The weight and the dimensional changes during the reaction-bonding process were recorded with a thermobalance (TGA) and a dilatometer (TDA). Phase compositions were determined by X-ray diffractometry (XRD), and microstructures were studied by scanning electron microscopy (SEM). Densities of reaction-bonded specimens were estimated by Archimedes' principle of volume displacement. Fracture strength and Young's modulus were measured at room temperature in a universal testing machine in four-point bending (20/40 mm span). Only a few test specimens (dimensions: 55 × 6 × 2 mm^3) were prepared.

3 Results and Discussion

3.1 Specimen preparation

As can be seen in Fig. 1, the particle size was considerably reduced after milling and there are no large, flat agglomerates present. These micron-sized, round-shaped particles favour a more homogeneous particle distribution in the powder compacts and facilitate the infiltration of fibre tows. A number of as-received, spherical Al–Si alloy particles are shown in the left micrograph.

The milling result was also checked by BET specific surface area measurements, which gave 2·7 m^2/g before milling and 8·8 m^2/g after milling.

The bulk density of the slip cast green bodies was 58·0% of theoretical density (TD). Presumably, the green density of the matrix in the fibre wound composites was slightly less, due to non-optimized particle packing. By light microscope studies, no cracks could be found in the green composites.

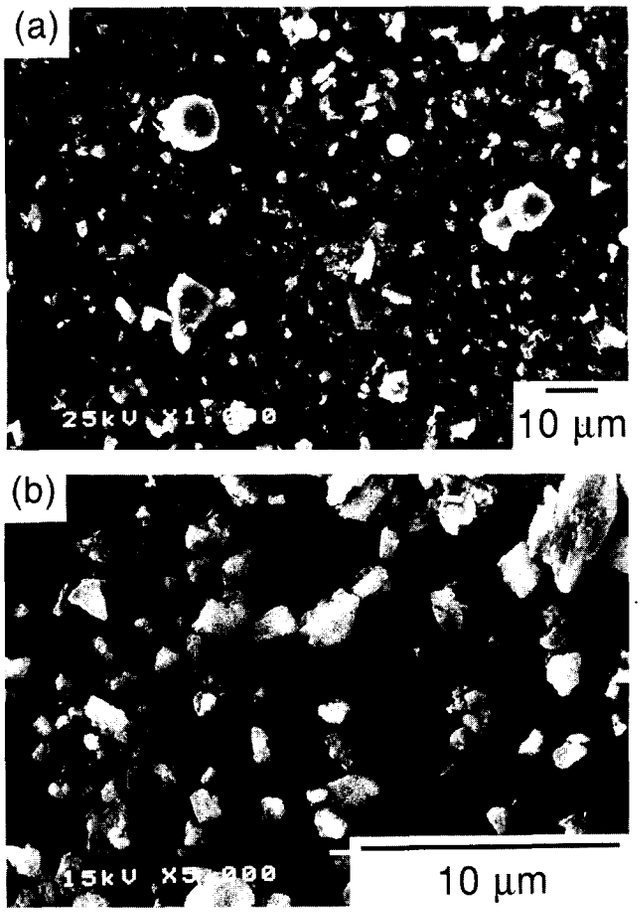

Fig. 1. Scanning electron micrographs of particles from the batch before (a) and after milling (b).

3.2 Oxidation/reaction-bonding behaviour

Thermogravimetry (TGA) and dilatometry (TDA) were used to determine the oxidation and reaction-bonding behaviour of slip cast, green bodies. In Fig. 2, the dimensional change, degree of oxidation and oxidation rate during the reaction-bonding cycle are shown.

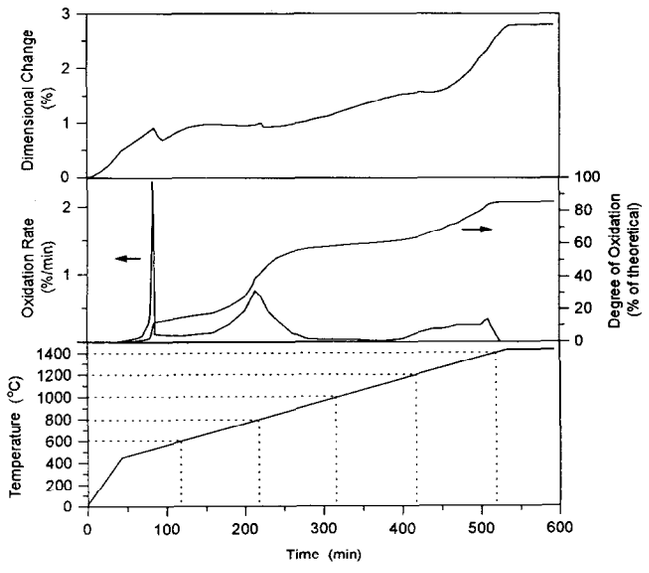

Fig. 2. Dimensional change, degree of oxidation and oxidation rate of a slip cast and burned out powder compact (without fibres) as a function of the reaction-bonding cycle, in flowing air. The total cycle time, including cooling, was 10 h.

The oxidation rate curve in Fig. 2, shows a sharp oxidation peak at 528°C, where surface oxidation of solid Al particles takes place. This reaction is strongly exothermal and probably causes local temperature increase. Since the alloy starts to melt at 577°C, this intermittent increase is expected to be high enough to partly melt the alloy, enabling a certain particle rearrangement. This may explain the minor shrinkage in the TDA at 530°C. In addition, the fine-grained Al_2O_3 that is formed reacts with the added MgO to form spinel ($MgAl_2O_4$), which presumably further favours the oxidation of Al in this temperature region.[17] Approximately 15% of the Al in the alloy appears to oxidize by solid state/gas reaction.

After further heating, the oxidation of Al slows down considerably. At about 680°C, though, the process accelerates, with an oxidation rate maximum at 797°C. The thermal expansion of the melt presumably results in a rupture of the oxide shell so that the melt leaks out, resulting in a more rapid oxidation.[12,18] This causes, once again, a shrinkage of the powder compact because of the particle rearrangement. This is consistent with the dilatometer analysis, with the shrinkage starting at 680°C, followed by an intermediary expansion peak at 805°C, then a small drop, before the expansion continues.

As the Al in the melt is consumed, the phase composition of the alloy is shifted towards the Si corner.[14] The liquidus temperature (when also the Si grains melt) increases gradually. An oxidation rate of 0·2 %/min (based on TGA) for the Al corresponds to an increase in the liquidus temperature of approximately 1°C/min. The Si will thus be supersaturated and precipitate, which has been verified by calculations. Consequently, the primary solid Si grains will not dissolve at the liquidus temperature of A175/Si25 of 760°C.

The increasing oxidation rate at ~ 1180°C indicates that Si begins to oxidize in order to form α-cristobalite (SiO_2). In spite of the fact that there is a large volume increase involved when Si oxidizes (114%), the TDA shows no expansion from 1200 up to 1240°C. One possible explanation is that the previously formed, fine α–Al_2O_3 crystals to some extent sinter. Above 1240°C, however, the oxidation of Si prevails and the expansion curve rises steeply as expected until all the Si has been oxidized. The small oxidation rate peak at 1395°C is related to the melting temperature of Si (1410°C), which may be lowered due to impurities. It is interesting to note the high degree of conversion (85·5% of the theoretical weight gain), implying that less than 15% of the alloy was

oxidized during milling. This is one of the significant advantages when employing an alloy instead of pure Al (for which up to 40 wt% premature oxidation has been reported[11,18]). There is another advantage during reaction-bonding due to the sluggish oxidation of Si: The homogeneously distributed Si in the alloy, which encloses the reactive Al, improves the oxidation controllability and the oxidation rate can thus be increased.

All oxidation experiments were carried out in air. During this process a large amount of oxygen is consumed. According to a rough estimate (assumptions: an average pore volume of 40% in the green bodies, pores filled with oxygen batchwise at an average oxidation temperature of 800°C), the pore network has to be refilled 17 000 times with oxygen from the surrounding air to completely oxidize the specimens. This leads to a substantial reduction of the partial oxygen pressure, especially in the interior part, since the surface layer reacts with most of the inflowing oxygen. However, to avoid a runaway oxidation because of the strongly exothermal nature of the oxidation reaction, low partial oxygen pressure is necessary.

The conversion to mullite ($3Al_2O_3 + 2SiO_2 \rightarrow Al_6Si_2O_{13}$) begins below 1400°C. Table 1 shows the resulting crystalline phases before and after oxidation at 1430°C in flowing air.

Practically all Si and SiO_2 have reacted with Al_2O_3 to form mullite already after 5 min at 1430°C. In addition, an intermediate phase of cordierite ($2MgO{\cdot}2Al_2O_3{\cdot}5SiO_2$) has formed. Cordierite is an undesirable final product, since two of the ternary eutectic compositions including cordierite in the $MgO–Al_2O_3–SiO_2$ system melt at 1345 and 1360°C, respectively. Fortunately, the cordierite turns into mullite and a Mg-, Al-spinel during extended heating at 1430°C. Yet to be explored is if cordierite favours the mullitalization process.

According to Table 1, after oxidation/reaction-bonding at 1430°C for 60 min in flowing air, the predominant phase was mullite, but there was also some Al_2O_3, due to the surplus alumina added, together with traces of cordierite. The total linear dimensional change for the specimen above was 2% in expansion.

3.3 Microstructure and mechanical properties of composites

Figure 3 shows micrographs of sapphire fibre reinforced mullite, reaction-bonded at three different temperatures. The effect of increasing the maximum reaction temperature can clearly be observed. First, the obvious increase of the density of the matrices: the density was after reaction-bonding at 1430°C (5 min) 65·6%, 1430°C (60 min) 66·5%, 1500°C (60 min) 80·2% and at 1600°C (60 min) 94·1% of theoretical density. The 1600°C matrix had only closed porosity. This can also be seen by comparing the SEM micrographs, where the open, fine-distributed pore network in Figs 3(a–d) have changed into enlarged close pores in Figs 3(e,f).

Images of the sapphire fibre/matrix interfaces in Fig. 3(b,d) indicate that there are spaces between the fibres and the matrices, whereas in Fig. 3(f), no space can be observed. Instead, surrounding cracks in the matrix are seen. These phenomena are due to the expansion coefficient mismatch of alumina ($8{\cdot}8 \times 10^{-6}$ K^{-1}) and mullite ($5{\cdot}3 \times 10^{-6}$ K^{-1}). Thus, during cooling, the sapphire fibres shrink more than the mullite matrices, causing a widening of the interface spaces. According to calculations, the space width should theoretically be 0·35 μm. At the higher temperature (Fig. 3(f)), the matrix may react with the fibres to form a strong bond. The cooling stresses then lead to cracking of the adjacent matrix and even of the fibres.

One role of the fibres is to increase the fracture toughness of the material.[19] As suggested by Davis *et al.*,[20] the interfacial debonding energy should be about one quarter of the fibre fracture energy, resulting in high-energy sliding when the fibres are pulled out. Figure 4 shows a sapphire fibre pull-out in a matrix of mullite, but whether this composite, reaction-bonded at 1430°C for 60 min, has the appropriate energy ratio has not yet been examined. A possibility is to coat the fibres with an interfacial, debonding layer, for instance ZrO_2,[20,21] and thus enable sintering of the composite at higher temperatures.

In Fig. 5, an ALMAX fibre reinforced mullite composite is shown. For all composites based on ALMAX fibres, the reaction-bonding cycle was

Table 1. Crystalline phases of the green and the reaction-bonded matrices, by X-ray diffraction.

Temp. (°C)	*Time (min)*	*$Al_6SiO_2O_{13}$ (mullite)*	*Al_2O_3*	*Al*	*Si*	*SiO_2*	*MgO*	*$2MgO{\cdot}2Al_2O_3{\cdot}5SiO_2$ (cordierite)*
Green body		m	w	s	s	w	vw	—
1430	5	s	w/m	—	—	vw	—	w
1430	60	s	w	—	—	—	—	vw

s = strong; m = medium; w = weak; vw = very weak.

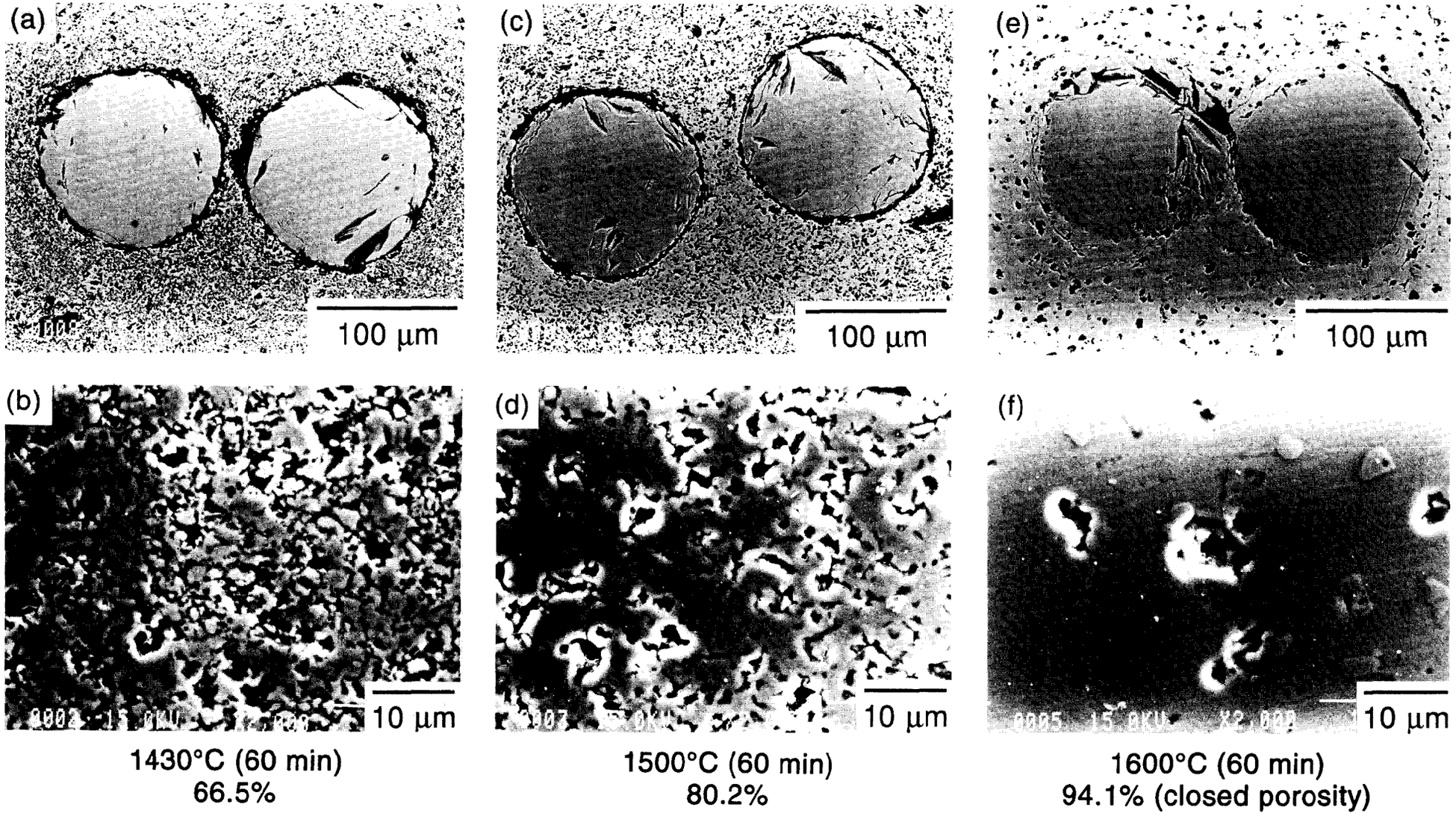

Fig. 3. Scanning electron micrographs of sapphire fibre reinforced mullite, reaction-bonded at 1430 (a, b), 1500 (c, d) and 1600°C (e, f), respectively, for 60 min. The graphs underneath are close-ups of the matrices above.

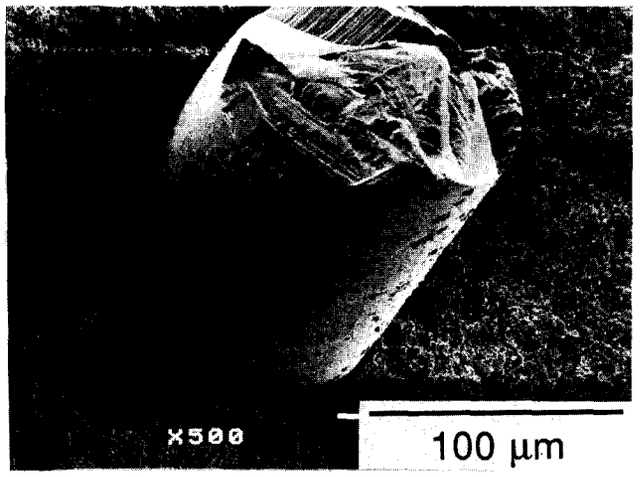

Fig. 4. Scanning electron micrograph of the fracture of a sapphire fibre reinforced mullite specimen, reaction-bonded at 1430°C for 60 min, showing a fibre pull-out.

limited to 1430°C for 5 min. This because the polycrystalline ALMAX fibres may degrade at elevated temperatures, as mentioned previously.

From the close-up (Fig. 5(b)), it is clear that the slurry has properly infiltrated the fibre tows and no fibres are in contact with each other. In addition, no cracks can be detected. The absence of cracks is probably due to the internal volume

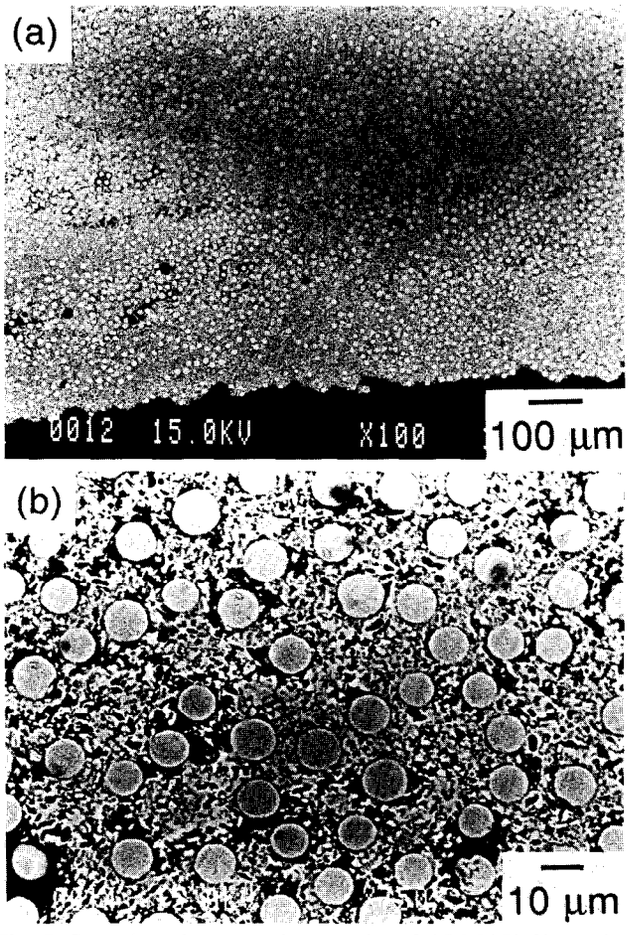

Fig. 5. Scanning electron micrographs of ALMAX fibre reinforced mullite, prepared by slurry infiltration/fibre winding followed by reaction-bonding at 1430°C for 5 min. The fibres are approximately 10 μm in diameter.

expansion of the matrix on oxidation, which reduces the fibre/matrix stresses. Unfortunately, the overview graph shows regions where there are almost no fibres present, indicating that too much slurry has covered the tows during winding and hence obstructed a homogeneous fibre distribution.

The fracture behaviour of an as-reaction bonded ALMAX fibre/mullite matrix composite is illustrated in Fig. 6. As the test specimens were not machined, this test only gives an indication of the strength potential for these composites. For the charted one, which was reaction-bonded at 1430°C for 5 min, the strength was 120 MPa. As can be seen, there was no catastrophic failure; on the contrary, a partial load-transfer took place. Even after testing, the broken parts held together. The Young's modulus was calculated for the first straight slope; with a thickness of the specimen of 2 mm it was roughly 90 GPa.

4 Conclusion

Composites of reaction-bonded long-fibre reinforced mullite were prepared by means of a new reaction-bonding technique. Both the technique, in which an Al–Si alloy in a powder compact during oxidation converts to mullite, as well as the preparation of the composites via a slurry route were demonstrated.

Starting with an Al–Si alloy, instead of Al and Si as separate components, resulted in a more effective milling, a better distribution of the two reactants, less undesired oxidation during milling and improved control of the oxidation during the reaction-bonding cycle. Furthermore, there was neither Si nor SiO_2 in the final matrix material, reaction-bonded at 1430°C for 1 h.

The long-fibres, including also fibre tows, were properly infiltrated by the Al–Si-based slurry. After reaction-bonding at 1430°C for 5 min, the

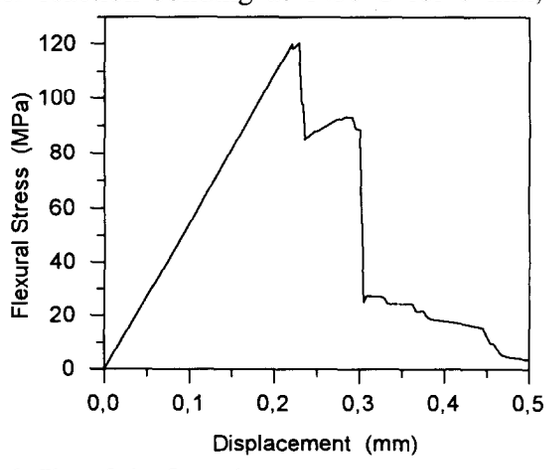

Fig. 6. Plot of the flexural stress at room temperature as a function of the displacement of an ALMAX fibre reinforced mullite test specimen, reaction-bonded at 1430°C for 5 min.

ALMAX-based composites showed no matrix cracks. The flexural test gave non-catastrophic failure characteristics. For the sapphire-based composites, reaction-bonded at 1430 and 1500°C, for 1 h, there were void spaces between the fibres and the mullite, due to a thermal expansion mismatch on cooling.

Acknowledgements

We wish to thank Lars Eklund for all SEM micrographs, Annika Kristoffersson for assistance in fibre winding and Robert Pompe for valuable discussions and constructive criticism of this paper.

References

1. Butler, E. G. & Lewis, M. H., Prospects for ceramics in airborne gas turbine engines. In *Proceedings of the 4th International Symposium on Ceramic Materials and Components for Engines*, eds R. Carlsson, T. Johansson & L. Kahlman, Elsevier Applied Science, London, 1991, pp. 32–49.
2. Brandt, J., Rundgren, K., Pompe, R., Swan, H., O'Meara, C., Lundberg, R. & Pejryd, L., SiC continuous fiber-reinforced Si_3N_4 by infiltration and reaction bonding. *Ceram. Eng. Sci. Proc.*, **13** (1992) 622–31.
3. Kristoffersson, A., Warren, A., Brandt, J. & Lundberg, R., Reaction bonded oxide composites. In *Proceedings of the 6th European Conference on Composite Materials (EACM), High Temperature Ceramic Matrix Composites*, eds R. Naslain, J. Lamon & D. Doumeingts, Woodhead Publishing Ltd, Abington Cambridge, UK, 1993, pp. 151–9.
4. Aksay, I. A., Dabbs, D. M. & Sarikaya, M., Mullite for structural, electronic, and optical applications. *J. Am. Ceram. Soc.*, **74** (1991) 2343–58.
5. Dokko, P. C., Pask, J. A. & Mazdiyasni, K. S., High-temperature mechanical properties of mullite under compression. *J. Am. Ceram. Soc.*, **60** (1977) 150–5.
6. Sacks, M. D., Lee, H. & Pask J. A., A review of powder preparation methods and densification procedures for fabricating high density mullite. In *Proceedings of the International Conference on Mullite*, Vol. 6, American Ceramic Society, Westerville, OH, USA, 1990, pp. 167–207.
7. Ko, F. K., Preform fiber architecture for ceramic-matrix composites. *Am. Ceram. Soc. Bull.*, **68** (1989) 401–14.
8. Brandt, J. & Lundberg, R., Synthesis of mullite materials by oxidation of metal alloy powder compacts. In *Third Euro-Ceramics, Vol. 1 Processing of Ceramics*, eds P. Duran & J. F. Fernández, Faenza Editrice Ibérica S.L., Spain, 1993, pp. 169–76.
9. Milling of brittle and ductile materials. *Metals Handbook*. Vol 7, 9th Edition, ASM International, Materials Park, OH, 1984, 56–70.
10. Claussen, N., Le, T. & Wu, S., Low-shrinkage reaction-bonded alumina. *J. Eur. Ceram. Soc.*, **5** (1989) 29–35.
11. Wu, S. & Claussen, N., Fabrication and properties of low-shrinkage reaction-bonded mullite. *J. Am. Ceram. Soc.*, **74** (1991) 2460–3.
12. Claussen, N., Wu, S. & Holz, D., Reaction bonding of aluminium oxide (RBAO) composites: processing, reaction mechanisms and properties. *J. Eur. Ceram. Soc.*, **14** (1994) 97–109.
13. Thompson, I. & Witt, M. C., Fabrication of continuous fibre ceramic matrix composites via slurry routes. In *British Ceramic Proceedings No. 49, Special Ceramics 9*, The Institute of Ceramics, Stoke-on-Trent, 1992, pp. 269–78.
14. Specific metals and alloys. *Metals Handbook*, Vol 2, 10th Edition, ASM International, Materials Park, OH, 1990, pp. 124.
15. Corman, G. S., High-temperature creep of some single crystal oxides. *Ceram. Eng. Sci. Proc.*, **12** (1991) 1745–66.
16. Haggerty, J. S., Wills, K. C. & Sheehan, J. E., Growth and properties of single crystal oxide fibres. *Ceram. Eng. Sci. Proc.*, **12** (1991) 1785–801.
17. Newkirk, M. S., Urquhart, A. W. & Zwicker, H. R., Formation of Lanxide™ ceramic composite materials. *J. Mater. Sci.*, **1** (1986) 81–9.
18. Wu, S., Holz, D. & Claussen, N., Mechanism and kinetics of reaction-bonded aluminium oxide ceramics. *J. Am. Ceram. Soc.*, **76** (1993) 970–80.
19. *International Encyclopedia of Composites*. Vol. 1, eds Lee, S. M., VCH Publishers, Inc., New York, 1990, pp. 267–77 and 297–318.
20. Davis, J. B, Löfvander, J. P. A. & Evans, A. G., Fiber coating concepts for brittle-matrix composites. *J. Am. Ceram. Soc.*, **76** (1993) 1249–57.
21. Hay, R., Fiber–matrix interfaces for oxide fiber-oxide matrix composites. In *Proceedings of the 6th European Conference on Composite Materials, High Temperature Ceramic Matrix Composites*, eds R. Naslain, J. Lamon & D. Doumeingts, Woodhead Publishing Ltd, Abington Cambridge, UK, 1993, pp. 385–9.